Somatostatin and parvalbumin inhibitory synapses onto hippocampal pyramidal neurons are regulated by distinct mechanisms

Meryl E. Horn[a,b] and Roger A. Nicoll[a,c,1]

[a]Department of Cellular and Molecular Pharmacology, University of California, San Francisco, CA 94158; [b]Neuroscience Graduate Program, University of California, San Francisco, CA 94158; and [c]Department of Physiology, University of California, San Francisco, CA 94158

Contributed by Roger A. Nicoll, December 7, 2017 (sent for review November 8, 2017; reviewed by Carleton Goold and Ivan Soltesz)

Excitation–inhibition balance is critical for optimal brain function, yet the mechanisms underlying the tuning of inhibition from different populations of inhibitory neurons are unclear. Here, we found evidence for two distinct pathways through which excitatory neurons cell-autonomously modulate inhibitory synapses. Synapses from parvalbumin-expressing interneurons onto hippocampal pyramidal neurons are regulated by neuronal firing, signaling through L-type calcium channels. Synapses from somatostatin-expressing interneurons are regulated by NMDA receptors, signaling through R-type calcium channels. Thus, excitatory neurons can cell-autonomously regulate their inhibition onto different subcellular compartments through their input (glutamatergic signaling) and their output (firing). Separately, while somatostatin and parvalbumin synapses onto excitatory neurons are both dependent on a common set of postsynaptic proteins, including gephyrin, collybistin, and neuroligin-2, decreasing neuroligin-3 expression selectively decreases inhibition from somatostatin interneurons, and overexpression of neuroligin-3 selectively enhances somatostatin inhibition. These results provide evidence that excitatory neurons can selectively regulate two distinct sets of inhibitory synapses.

inhibition | parvalbumin | somatostatin | NMDA receptors | voltage-gated calcium channels

It is well known that excitatory and inhibitory brain activity is correlated in vivo in both spontaneous and sensory-evoked activity, in the hippocampus and the neocortex (1–4). Dysregulation of excitatory–inhibitory balance is thought to be associated with neurological disorders such as autism and schizophrenia (5, 6). While it has long been known that pharmacological inhibition of neuronal firing causes a decrease in inhibition onto excitatory neurons (7), the molecular basis underlying cell-autonomous homeostatic changes of inhibitory inputs remains unclear. Separately, while there has been progress in characterizing the molecular composition of the inhibitory postsynaptic density (8), the degree to which synapses formed by different types of inhibitory neurons differ in their composition is uncertain.

We have recently found that elimination of excitatory current in a pyramidal neuron (PN) causes a cell-autonomous decrease in inhibitory postsynaptic currents (IPSCs) onto that neuron (9). Xue et al. (10) showed that although changes in PN firing in the visual cortex lead to positively correlated changes in IPSCs from parvalbumin (PV)-expressing interneurons onto those PNs, PN firing does not change IPSCs from somatostatin (SOM)-expressing interneurons. Additionally, elimination of NMDA receptors (NMDARs), but not AMPA receptors (AMPARs), in PNs causes a decrease in IPSCs onto those cells (11), suggesting signaling through NMDARs is important for modulation of inhibitory inputs. While these studies indicate that excitatory neurons can alter their inhibitory inputs cell-autonomously, the mechanisms underlying this plasticity, and whether there are ways to specifically alter SOM synapses, are unclear.

By using optogenetic stimulation of either PV- or SOM-expressing interneurons, and measuring IPSCs onto PNs (PV-IPSCs or SOM-IPSCs), we show evidence for the distinct molecular composition, as well as distinct homeostatic regulatory pathways, governing the formation of these synapses. Altering neuroligin-3 (NLGN3) expression specifically affected SOM-IPSCs but not PV-IPSCs. PV-IPSCs were regulated by firing of the target neuron, a process dependent on L-type calcium channel (LTCC) current. Conversely, SOM-IPSCs were regulated by NMDARs, a process dependent on R-type calcium channel (RTCC) current. Together, this work shows that PNs are capable of cell-autonomously regulating different sources of inhibition in distinct ways.

Results

We crossed either PV-IRES-Cre or SOM-IRES-Cre mice with Ai32 (lox-stop-lox-ChR2) mice, leading to Cre-mediated excision of the floxed stop signal and expression of ChR2 selectively in either PV- or SOM-expressing neurons (PV:ChR2 or SOM:ChR2 mice) (Fig. 1*A*). We used biolistic transfection of organotypic hippocampal slices at day 1 in vitro (1DIV) with the goal to selectively modulate PN gene expression, as this technique ensures very low transfection efficiency. IPSC recordings at 0 mV were made from pairs of transfected–untransfected CA1 PNs between 2 and 3 wk in vitro. We used PV:ChR2 mice to record light-evoked PV-IPSCs and SOM:ChR2 mice to record SOM-IPSCs.

Despite the prolific use of PV and SOM-Cre mice, little is known (12) regarding whether these sets of synapses are composed of different postsynaptic proteins. Therefore, we first set out to determine whether the canonical inhibitory postsynaptic proteins showed selective effects for PV- vs. SOM-IPSCs. We

Significance

Stable brain functioning requires a balancing of excitatory and inhibitory signaling, a phenomenon known as "excitatory–inhibitory balance" or homeostasis. Dysregulation of homeostasis is thought to be linked to diseases such as autism and schizophrenia, although the molecular mechanisms underlying this process remain unclear. Here, we elucidate the ways excitatory neurons can regulate their inhibitory synapses, finding that neurons can regulate different forms of inhibitory input through distinct molecular pathways. We also found evidence that these different forms of inhibitory input depend on different postsynaptic inhibitory proteins. Thus, while it has long been known that different types of inhibitory neurons shape activity in different ways, this study clarifies how these forms of inhibition may be differentially regulated.

Author contributions: M.E.H. and R.A.N. designed research; M.E.H. performed research; M.E.H. contributed new reagents/analytic tools; M.E.H. and R.A.N. analyzed data; and M.E.H. wrote the paper.

Reviewers: C.G., Novartis Institutes for BioMedical Research; and I.S., Stanford University.

The authors declare no conflict of interest.

[1]To whom correspondence should be addressed. Email: Roger.Nicoll@ucsf.edu.

This article contains supporting information online at www.pnas.org/lookup/suppl/doi:10.1073/pnas.1719523115/-/DCSupplemental.

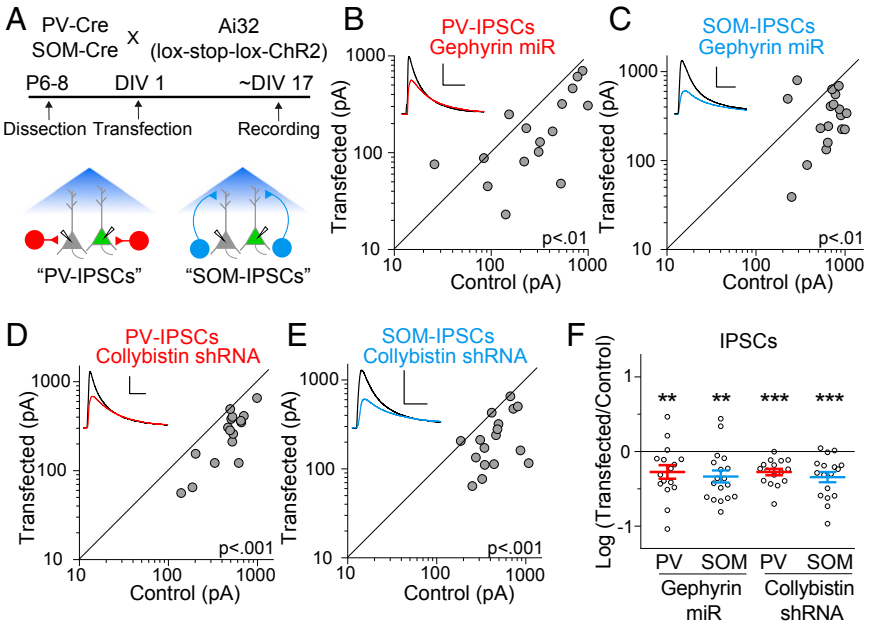

Fig. 1. Reduction of gephyrin and collybistin affect both PV- and SOM-IPSCs. (*A*) Model showing mouse breeding scheme, experimental timelines, and patch-clamp configuration. (*B*) Scatter plots show amplitudes of IPSCs recorded from pairs of gephyrin miR transfected and control cells at ~17DIV in PV:ChR2 mice. (*C*) Same as in *B* but with SOM:ChR2 mice. (*D*) Same as in *B* but transfecting with collybistin shRNA. (*E*) Same as in *D* but with SOM:ChR2 mice. (*F*) Summary plot showing IPSCs as a $\log_{10}$ of the ratio in transfected and control neurons, mean ± SEM (gephyrin miR: PV-IPSCs $P < 0.01$, $n = 16$; SOM-IPSCs, $P < 0.01$, $n = 18$; collybistin shRNA: PV-IPSCs $P < 0.001$, $n = 16$; SOM-IPSCs, $P < 0.001$, $n = 17$). Black sample traces are control and colored traces are transfected cells. (Scale bars: 200 pA and 40 ms.) $^{**}P < 0.01$, $^{***}P < 0.001$.

used several validated (*SI Materials and Methods* and Fig. S1) RNA-interference tools to test how reducing levels of gephyrin, collybistin, NLGN2, and NLGN3 impacts PV and SOM-IPSCs. Transfecting PNs with either a micro-RNA (miR) targeting gephyrin (Fig. 1 *B*, *C*, and *F*) or a shRNA against collybistin (Fig. 1 *D*–*F*) both led to similar reductions in PV-IPSCs and SOM-IPSCs. We then tested NLGN2 and NLGN3, the two isoforms of neuroligins found at inhibitory synapses (13, 14). We transfected PNs with a miR targeting NLGN2 and found that both PV-IPSCs (Fig. 2 *A* and *I*) and SOM-IPSCs (Fig. 2 *B* and *I*) were dramatically decreased.

Next, we transfected PNs with a miR targeting NLGN3. While transfecting PNs with the NLGN3miR did not significantly affect PV-IPSCs (Fig. 2 *C* and *I*), SOM-IPSCs were decreased (Fig. 2 *D* and *I*). To verify the specificity of NLGN3 for SOM-IPSCs, we overexpressed NLGN3 in combination with NLGN2miR. This should prevent the dimerization of the overexpressed NLGN3 with endogenous NLGN2 (15) and allow us to only look at the effects of NLGN3 homomers. We found that PV-IPSCs were reduced to a similar extent as the NLGN2miR on its own, suggesting that NLGN3 is not capable of enhancing these synapses (Fig. 2 *E* and *I*). However, overexpressing NLGN3 with NLGN2miR dramatically enhanced SOM-IPSCs (Fig. 2 *F* and *I*). We then tested whether overexpression of NLGN3 alone can enhance PV-IPSCs. This manipulation still failed to enhance, and in fact led to a decrease in, PV-IPSCs (Fig. 2 *G* and *I*). As expected, NLGN3 overexpression profoundly enhanced SOM-IPSCs (Fig. 2 *H* and *I*). Together, these results show that while both PV-IPSCs and SOM-IPSCs depend on gephyrin, collybistin, and NLGN2, SOM-IPSCs are selectively and profoundly regulated by NLGN3.

We then wanted to test whether there are also different plasticity pathways selective for PV- or SOM-IPSCs. As there is evidence that PV-IPSCs are regulated by the target neuron firing rate (10, 16), we aimed to test this directly by using CRISPR/Cas9 to target PN sodium channels. Hippocampal PNs express Nav1.2 and Nav1.6, and possibly trace amounts of Nav1.1 and Nav1.3 (17, 18). We therefore designed one guide RNA (gRNA) targeting Nav1.6 and one gRNA targeting a sequence present in Nav1.1, Nav1.2, and Nav1.3. We first tested whether PNs transfected with these gRNAs, along with Cas9 ("ΔNav"), were able to fire action potentials. We found that the majority (20/32) of transfected PNs fired no action potentials (Fig. 3*A*). In the 12/32 PNs that were still able to fire, we found that the action potentials had significantly slower rise times, decreased height, and decreased slopes (Fig. S2 *A*–*D*). We then measured the PV-IPSCs and found that they were significantly decreased in ΔNav cells (Fig. 3 *B* and *E*), while SOM-IPSCs showed no change (Fig. 3 *C* and *E*). These results support a model in which a cell-autonomous reduction of firing in PNs causes a decrease in PV-IPSCs but has no significant effects on SOM-IPSCs.

To test whether the mechanism through which neuronal firing regulates PV-IPSCs is dependent on LTCC, as they have been found to mediate forms of action potential-dependent excitatory homeostatic plasticity (19–22), we incubated slices transfected with ΔNav in 20 μM nifedipine, a specific inhibitor of LTCC. As this will block LTCC on both the transfected and the control cells, any remaining difference between the cells indicates that the decrease in PV-IPSCs is not dependent on LTCC signaling. However, in the presence of nifedipine no difference in the size of PV-IPSCs was seen between ΔNav cells and control cells (Fig. 3 *D* and *E*), suggesting an occlusion of the effect. Therefore, elimination of action potential firing causes a decrease in PV-IPSCs through a reduction in current from LTCC.

Finally, we sought to determine whether the nature of the decrease in PV-IPSCs in ΔNav cells was due to a reduction in the number of functional synapses (N), a reduction in presynaptic probability of release (P_r), or a reduction in the number of $GABA_A$ receptors ($GABA_AR$) at each synapse (q). We decided to use coefficient of variation (CV) analysis, a technique which uses the inherent IPSC amplitude variability from trace to trace to differentiate between changes in quantal content ($N \times P_r$) and size (q) between two simultaneously recorded neurons (see *SI Materials and Methods* for further description of this technique). We found that the decrease in PV-IPSCs represents a change in quantal content ($N \times P_r$) rather than quantal size (q) (Fig. 3*F*). To determine whether the decrease in PV-IPSCs in ΔNav cells is caused by altered P_r, we measured the paired-pulse ratio (PPR) of ΔNav and control cells. At no interval did we find a significant difference between the PPRs in ΔNav and control cells (Fig. S2*E*). Together, this indicates that the decrease in PV-IPSCs in ΔNav cells represents a change in N: an all-or-none loss in functional synaptic connections.

We were next interested in studying the factors controlling SOM-IPSCs. As SOM interneurons largely target dendrites (23) where excitatory synapses containing NMDARs are found, and alterations in NMDAR levels can regulate IPSCs (11), we decided to test whether NMDAR signaling specifically affects

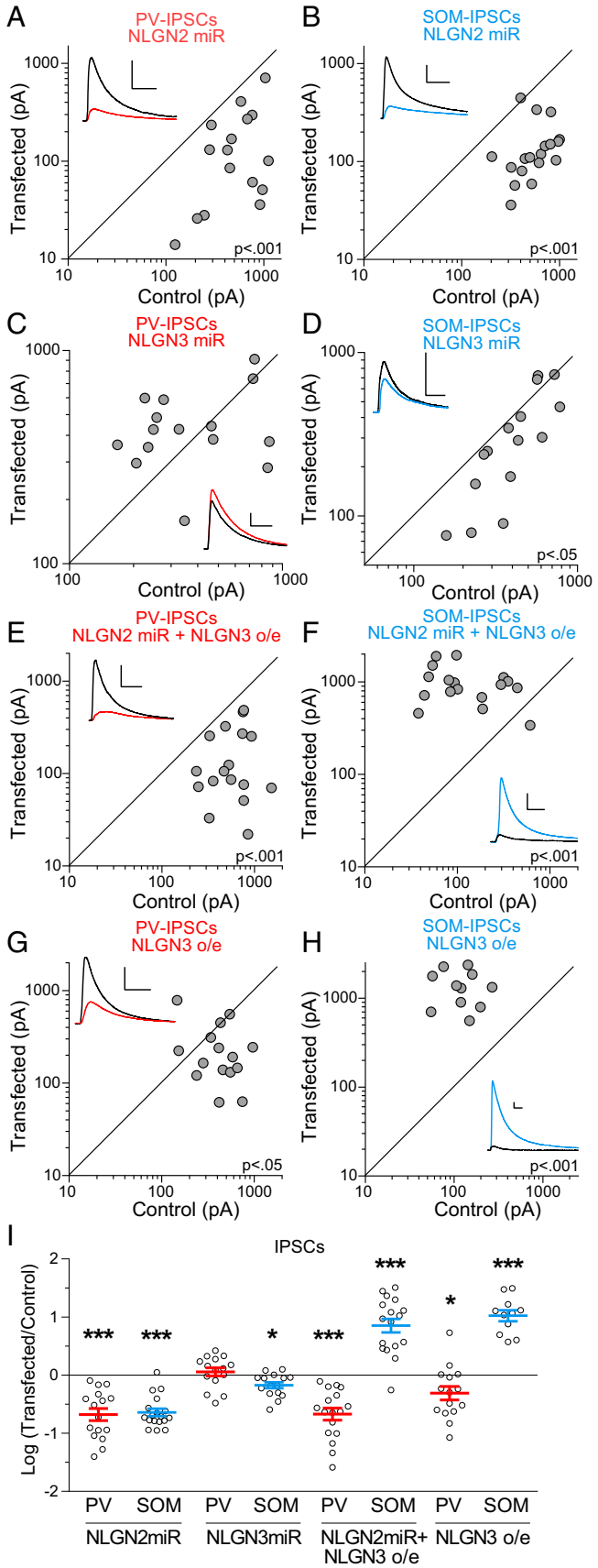

Fig. 2. NLGN2 reduction affects both PV- and SOM-IPSCs, while NLGN3 manipulations preferentially affect SOM-IPSCs. (*A*) Scatter plots show amplitudes of IPSCs recorded from pairs of NLGN2miR transfected and control cells at ~18DIV in PV:ChR2 mice. (*B*) Same as in *A* but in SOM:ChR2 mice. (*C*) Same as in *A* but transfecting with NLGN3miR. (*D*) Same as in *C* but in SOM:ChR2 mice. (*E*) Same as in *A* but expressing both NLGN2miR and overexpressing NLGN3. (*F*) Same as in *E* but in SOM:ChR2 mice. (*G*) Same as in *E* but only overexpressing NLGN3. (*H*) Same as in *G* but in SOM:ChR2 mice. (*I*) Summary plot showing IPSCs as a $\log_{10}$ of the ratio in transfected and control neurons, mean ± SEM (NLGN2miR: PV-IPSCs $P < 0.001$, $n = 16$, SOM-IPSCs, $P < 0.001$, $n = 18$; NLGN3miR: PV-IPSCs $P > 0.05$, $n = 15$, SOM-IPSCs, $P < 0.05$, $n = 15$; NLGN2miR + NLGN3 o/e: PV-IPSCs $P < 0.001$, $n = 17$, SOM-IPSCs $P < 0.001$, $n = 17$; NLGN3 o/e: PV-IPSCs $P < 0.05$, $n = 15$, SOM-IPSCs $P < 0.001$, $n = 11$). Black sample traces are control and colored traces are transfected cells. (Scale bars: 200 pA and 40 ms.) *$P < 0.05$, ***$P < 0.001$.

SOM-IPSCs. We therefore used CRISPR/Cas9 to target the obligatory NMDAR subunit, GluN1 ("ΔGluN1"). We used one of two different gRNAs, both previously validated (24, 25). We found robust reductions of NMDAR currents with both gRNAs (Fig. S3 *A* and *B*) and, as expected, greater reductions in NMDAR current were observed with more days posttransfection (Fig. S3*C*), indicating that any residual current is due to slow NMDAR turnover. We found no significant differences in NMDAR current remaining between the gRNAs (Fig. S3*B*), so we combined the datasets. There was no change in PV-IPSCs in ΔGluN1 cells (Fig. 4 *A* and *H*). However, we found a significant reduction in SOM-IPSCs in transfected PNs (Fig. 4 *B* and *H*).

To determine the mechanism through which NMDARs regulate SOM-IPSCs, we incubated slices in 200 μM D-APV, a competitive NMDAR antagonist which prevents glutamate binding to the NMDAR. Because the inhibitor will act on the control cells, we can use this experiment to determine whether the reduction in SOM-IPSCs in the ΔGluN1 cell is due to glutamate binding to the NMDAR. We found that this treatment occluded the decrease in SOM-IPSCs (Fig. 4 *C* and *H*), indicating a requirement for both glutamate binding to the NMDAR and, presumably, the subsequent NMDAR-dependent depolarization. Next, to determine explicitly whether ionotropic current through the NMDAR is necessary for this form of plasticity, we incubated slices in 100 μM MK-801, an NMDAR pore blocker. This, too, also occluded the decrease in SOM-IPSCs in ΔGluN1 cells (Fig. 4 *D* and *H*). Finally, we attempted to rescue SOM-IPSCs by expressing GluN1 N616R, a mutant subunit impermeable to calcium (26). For these experiments we switched to "GluN1 gRNA #3," which targets an intron–exon junction of the *Grin1* gene so it would not target the rescue construct (Fig. S3*D*). We then coexpressed ΔGluN1 with GluN1 N616R. We confirmed the presence of GluN1 N616R by measuring NMDAR current at −70 mV, as these channels are insensitive to magnesium (Fig. S3*E*). Unexpectedly, this manipulation rescued the SOM-IPSCs (Fig. 4 *E* and *H*), indicating that calcium influx through NMDARs is unnecessary in regulating SOM-IPSCs.

To test whether other sources of calcium are required, we inhibited either LTCC or RTCC, which are both found on spines (27, 28). While incubation with 20 μM nifedipine did not block the relative decrease in SOM-IPSCs in ΔGluN1 transfected cells (Fig. 4 *F* and *H*), incubation with 500 nM SNX-482, an RTCC blocker, successfully occluded the decrease (Fig. 4 *G* and *H*). This suggests a pathway wherein NMDAR-driven sodium influx regulates SOM-IPSCs through RTCC. We then used CV analysis on the SOM-IPSCs in ΔGluN1 cells and found that this decrease represents a change in quantal content, rather than quantal size (Fig. 4*I*). We also found no change in the PPR between the ΔGluN1 and control cells at any interval tested (Fig. S3*F*). Together, this suggests that the decrease in SOM-IPSCs in ΔGluN1 cells represents an all-or-none loss in functional synaptic connections.

It occurred to us that the increase of SOM-IPSCs following overexpression of NLGN3 (Fig. 2*F*) might be due to an indirect effect of NLGN3 on NMDARs, as NLGN3 is known to localize to excitatory synapses (13). However, NMDAR-mediated currents were not enhanced in NLGN3 + NLGN2miR

NEUROSCIENCE

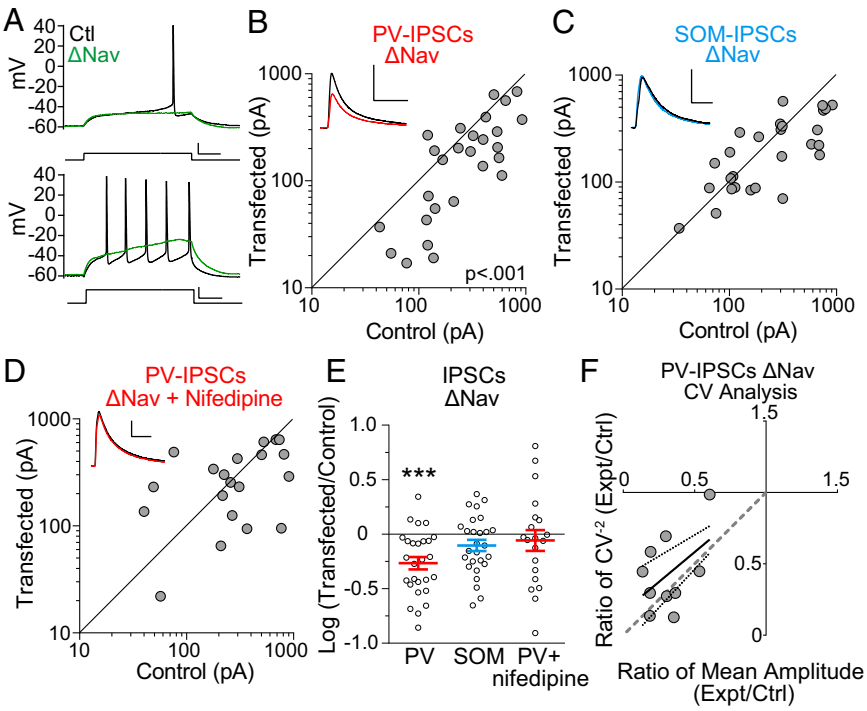

Fig. 3. PV-IPSCs are regulated by action potential firing through LTCC signaling. (*A*) Sample traces showing control (black) and ΔNav transfected cell (green) with current pulses to elicit a single (*Top*) and multiple (*Bottom*) action potentials in the control cell. (Scale bars: 100 pA and 100 ms.) (*B*) Scatter plots show amplitudes of optically evoked IPSCs recorded from pairs of ΔNav and control cells at ~17DIV in PV:ChR2 mice. (*C*) Same as in *B* but with SOM:ChR2 mice. (*D*) Same as in *B* but slices were incubated in 20 μM nifedipine from time of transfection to recording. (*E*) Summary plot showing IPSCs as a $\log_{10}$ of the ratio between transfected and control neurons, mean ± SEM (PV-IPSCs, $P < 0.001$, $n = 27$; SOM-IPSCs, $P > 0.05$, $n = 27$; PV-IPSCs + nifedipine, $P > 0.05$, $n = 20$). (*F*) CV analysis of control/ΔNav neuron pairs. CV^{-2} graphed against ratio of mean amplitude within each pair. Results along the horizontal y = 1 line are consistent with change in quantal size, and results along gray dashed identity (45°) line are consistent with change in quantal content. Small solid and dashed lines indicate linear regression line and 95% confidence intervals, respectively. Black sample traces are control and colored traces are transfected cells. (Scale bars in *B–E*: 200 pA and 40 ms.) ***$P < 0.001$.

cells (Fig. S3*G*). Therefore, the effect of NLGN3 on SOM-IPSCs likely represents a direct effect at inhibitory synapses.

Discussion

These results provide evidence that synapses formed by PV- and SOM-positive inhibitory neurons can be regulated in distinct ways (see model summarizing differences in Fig. S4). We show that NLGN3 specifically regulates synapses formed by SOM-expressing neurons, suggesting different molecular compositions between synapses formed by PV- and SOM-expressing cells. We found that PV- and SOM-IPSCs share a requirement for gephyrin, collybistin, and NLGN2. The fact that NLGN2 is required for SOM-IPSCs was surprising, given the fact that PV-unitary IPSCs (uIPSCs) but not SOM-uIPSCs are decreased in the NLGN2 knockout mouse (12). In that study, GIN (GFP-expressing inhibitory neurons) mice were used to identify SOM neurons, and SOM-uIPSC recordings were made from layer 2/3 of the somatosensory cortex. It is therefore possible that there is a difference in the SOM-expressing cells being activated, or that cells have a differential dependence on NLGN2 depending on the brain region.

We find that reduction of NLGN3 selectively reduces SOM-IPSCs and that overexpression of NLGN3 leads to a profound enhancement of SOM-IPSCs and a decrease of PV-IPSCs. It is possible that this decrease in PV-IPSCs is due to the fact that there is a limited amount of $GABA_AR$ in the PNs, which are incapable of supporting the enhancement of SOM-IPSCs while maintaining normal levels of PV-IPSCs. Or, NLGN3 could be actively suppressing PV-IPSCs. In NLGN3 knockout mice PV-IPSCs onto hippocampal PNs are unchanged, while CCK-IPSCs are increased (29). Together, this suggests that NLGN3 can have opposite effects on dendritic vs. somatic inhibition and is consistent with the fact that electrically induced IPSCs onto PNs in the hippocampus are unchanged after reduction of NLGN3 (30, 31). This study shows that a lack of effect on electrically induced IPSCs does not mean there are not profound effects on interneuron subtype-specific synapses.

Despite the fact that PV and SOM-Cre lines label heterogeneous populations (32, 33), several reports have demonstrated different functions of PV- vs. SOM-expressing interneurons in behavioral paradigms (34–37). Given this, and the role PV-expressing cells have been shown to play in action potential-dependent homeostasis (10, 16), we chose to use PV and SOM-Cre lines to further untangle the interneuron subclass-specific roles in GABAergic homeostasis, which has traditionally been studied by examining miniature IPSCs (mIPSCs) alone. Here, we show that the output of PNs (action potential firing) regulates PV-IPSCs, while the input of PNs (glutamatergic signaling via NMDARs) regulates SOM-IPSCs. This matches the known distribution of these inhibitory synapses: PV-positive interneurons largely target the soma and perisomatic dendrites, as well as the axon initial segment of PNs where action potentials are generated. SOM-positive interneurons generally target the more distal dendrites, which receive excitatory input. These targeting properties are found both in the hippocampus (23) and the neocortex (38) and are conserved in organotypic slices (39). It has recently been estimated that ~20% of spines contain inhibitory synapses (40). An intriguing possibility is that those SOM synapses colocalizing with excitatory synapses on spines are regulated by NMDARs.

We show that PV-IPSCs are regulated by action potential firing in a cell-autonomous manner. This agrees with what is known about the homeostatic regulation of IPSCs by neuronal firing in the neocortex, where it has been shown that pharmacological inactivation of firing with tetrodotoxin selectively

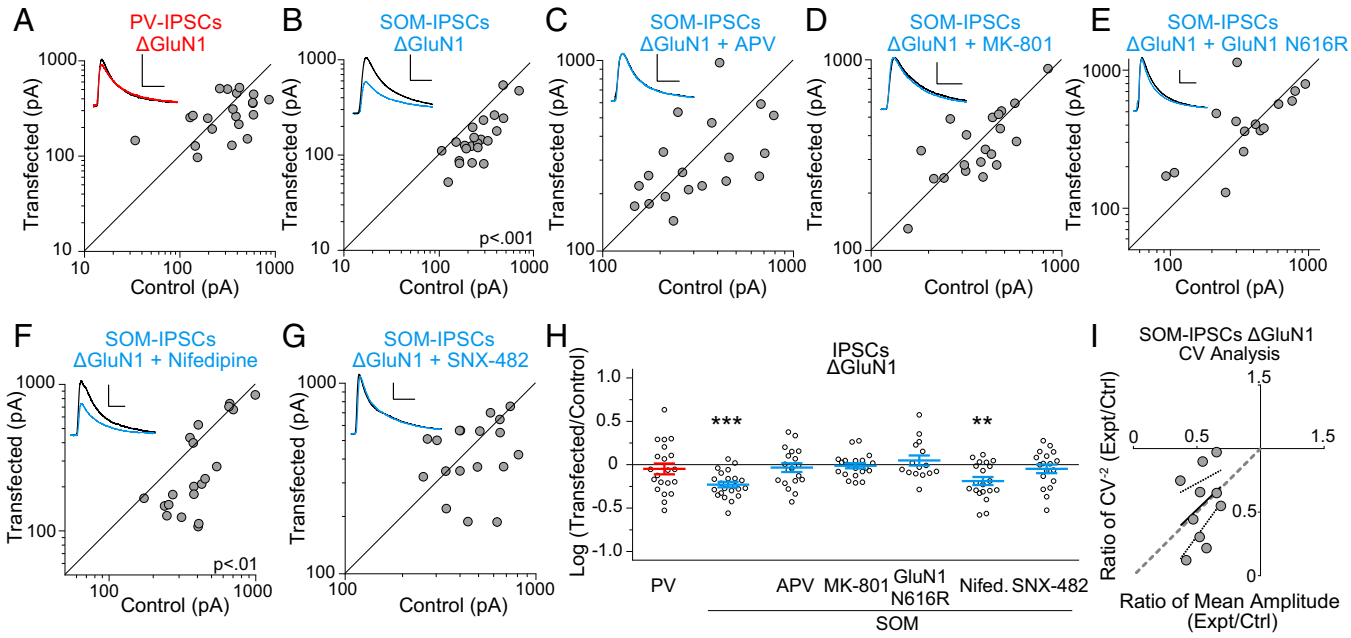

Fig. 4. Ablation of NMDA receptors selectively reduces SOM-IPSCs through RTCC signaling. (*A*) Scatter plots show amplitudes of IPSCs recorded from pairs of ΔGluN1 and control cells at ~17DIV in PV:ChR2 mice. (*B*) Same as in *A* but with SOM:ChR2 mice. (*C*) Same as in *B* but incubating slices in 200 μM D-APV. (*D*) Same as in *B* but incubating slices in 100 μM MK-801. (*E*) Same as in *B* but expressing both ΔGluN1 and GluN1 N616R. (*F*) Same as in *B* but incubating slices in 20 μM nifedipine from time of transfection to recording. (*G*) Same as in *B* but incubating slices in 500 nM SNX-482 from time of transfection to recording. (*H*) Summary plot showing IPSCs as a $\log_{10}$ of the ratio in transfected and control neurons, mean ± SEM (PV-IPSCs $P > 0.05$, $n = 21$; SOM-IPSCs, $P < 0.001$, $n = 22$; SOM-IPSCs + APV $P > 0.05$, $n = 19$; SOM-IPSCs + MK-801 $P > 0.05$, $n = 20$; SOM-IPSCs + GluN1 616R $P > 0.05$, $n = 15$; SOM-IPSCs + nifedipine $P < 0.01$, $n = 20$; SOM-IPSCs + SNX-482, $P > 0.05$, $n = 18$). (*I*) CV analysis of control/ΔGluN1 neuron pairs. CV^{-2} graphed against ratio of mean amplitude within each pair. Results along the horizontal y = 1 line are consistent with change in quantal size, and results along gray dashed identity (45°) line are consistent with change in quantal content. Small solid and dashed lines indicate linear regression line and 95% confidence intervals, respectively. Black sample traces are control and colored traces are transfected cells. (Scale bars: 100 pA and 40 ms.) $^{**}P < 0.01$, $^{***}P < 0.001$.

reduces connection probability of PV-uIPSCs, while SOM-uIPSCs remain unchanged (16), and, in vivo, cell-autonomous alterations of firing rate in PNs affects PV but not SOM-IPSCs onto those cells (10). We found that elimination of sodium channels does not reduce SOM-IPSCs (Fig. 3*C*), which suggests that local NMDAR-mediated spikes rather than back-propagating action potentials regulate these synapses, the majority of which likely target the distal dendrites in lacunosum moleculare (23).

We have found that chronic removal of NMDARs leads to selective decreases in SOM-IPSC strength. Several reports have previously shown that acute application of NMDA leads to a rapid increase in electrically induced IPSCs (41–43), suggesting that there are multiple time scales through which NMDARs can regulate IPSCs. Gu et al. (11) showed that loss of NMDARs leads to a decrease in mIPSC frequency (11). Expressing a calcium-impermeable NMDAR failed to rescue this effect, contrary to the mechanism reported here. It could be that different signaling pathways maintain inhibitory synapses at different developmental stages, as Gu et al. (11) used dissociated hippocampal cultures at 6DIV from embryonic mice, while the present study uses organotypic slices at 17DIV from postnatal day 6–8 mice. Dissociated hippocampal cultures from embryonic mice do show far lower RTCC transcript levels compared with adult hippocampi (44). The fact that in our study calcium entry through NMDAR is not sufficient to maintain the relative decrease in SOM-IPSCs following NMDAR removal (Fig. 4*G*) suggests that RTCCs are uniquely positioned to initiate the downstream mechanisms needed to regulate SOM-IPSCs, potentially through calcium microdomains.

LTCC signaling has been shown to be required for multiple forms of excitatory synapse homeostasis, through CaMKK, CaMKIV, and transcriptional activation (19–21). Potentially, PV-IPSCs are regulated by LTCC by similar transcriptional pathways. RTCC and LTCC also play a role in short-term plasticity of IPSCs in the visual cortex (45), by altering postsynaptic $GABA_AR$ expression through regulation of endocytosis and exocytosis. This suggests another possible downstream mechanism for the plasticity described here, though perhaps unlikely as the decreases in IPSCs here represent changes in quantal content.

We have found that both the decrease in PV-IPSCs in ΔNav cells and the decrease in SOM-IPSCs in ΔGluN1 cells represent changes in quantal content, rather than quantal size. This agrees with previous studies finding that eliminating AMPAR and NMDAR from PNs causes mostly a decrease in mIPSC frequency rather than amplitude (9), and that eliminating NMDAR from PNs causes only a decrease in mIPSC frequency but not amplitude (11). The decreases in PV-IPSCs and SOM-IPSCs described here may represent a decrease in the number of presynaptic release sites. Many studies have found roles for different mediators of retrograde signaling to inhibitory synapses, including brain-derived neurotrophic factor (46), nitric oxide (47), and endocannabinoids (48). Alternatively, the changes here may represent an all-or-none postsynaptic loss of $GABA_AR$, as the removal of postsynaptic proteins at excitatory synapses has been shown to cause all-or-none losses of glutamatergic receptors in an LTCC-dependent process (19).

Future studies may help determine the downstream mechanisms regulating GABAergic homeostasis, as well as whether there are particular subcategories of PV- and SOM-expressing cells important for these processes. While more work is needed to elucidate the mechanisms through which NLGN3 and other proteins affect excitatory–inhibitory balance, these results are intriguing given the links between both NLGN3 (49) and homeostatic plasticity (5) and autism. Considering the likelihood that different inhibitory neuron subtypes play different roles in circuit computations, it is not surprising that synapses from these neurons are regulated by the target neuron and by different processes.

Materials and Methods

Animals. To express ChR2 in PV or SOM-positive interneurons, PV-IRES-Cre mice or SOM-IRES-Cre mice were bred with Ai32 mice, a Cre-dependent ChR2 line. Mice that were either heterozygous or homozygous for each gene were used for dissection. Animals were housed according to the Institutional Animal Care and Use Committee guidelines at the University of California, San Francisco. Additional details for animals and other techniques can be found in *SI Materials and Methods*.

Slice Culture and Biolistic Transfection. Hippocampal organotypic slice cultures were prepared from mice at postnatal day 6–8. All constructs were transfected at 1DIV using biolistic transfection. Construct expression was confirmed by GFP and/or mCherry fluorescence. For the D-APV, MK-801, nifedipine, and SNX-482 experiments, slices were incubated from the time of transfection to the time of recording.

Electrophysiological Recording. Recordings were performed at 14–21DIV. Dual whole-cell recordings in area CA1 were done by simultaneously recording responses from a fluorescent transfected neuron and a neighboring untransfected control neuron. IPSCs were evoked using pulses of blue light [~5 ms, 0.05–1 mW, 10-s interstimulus interval (ISI)], through a 63× objective, adjusted to produce reliable IPSCs of 100–1,000 pA.

Statistical Analysis. All paired whole-cell data were analyzed using a two-tailed Wilcoxon matched-pairs signed rank test. N refers to number of pairs in all experiments except when otherwise noted. For nonpaired comparisons (Figs. S1–S3), a Mann–Whitney *U* test was used. Outliers in IPSC data were removed using a ROUT test, Q = 5% on the $\log_{10}$ transfected–control data, on all paired IPSC datasets (3 out of 403 pairs were removed).

ACKNOWLEDGMENTS. We thank V. S. Sohal and Z. A. Knight for providing the mice, M. Scanziani and K. Bender for manuscript comments, Q. A. Nguyen for performing the collybistin real-time PCR experiment in Fig. S1, M. Cerpas and D. Qin for technical assistance, and all members of the R.A.N. laboratory for comments on the manuscript. This work was supported by grants from the National Institute of Mental Health and the National Science Foundation.

1. Okun M, Lampl I (2008) Instantaneous correlation of excitation and inhibition during ongoing and sensory-evoked activities. *Nat Neurosci* 11:535–537.
2. Atallah BV, Scanziani M (2009) Instantaneous modulation of gamma oscillation frequency by balancing excitation with inhibition. *Neuron* 62:566–577.
3. Wehr M, Zador AM (2003) Balanced inhibition underlies tuning and sharpens spike timing in auditory cortex. *Nature* 426:442–446.
4. Wilent WB, Contreras D (2004) Synaptic responses to whisker deflections in rat barrel cortex as a function of cortical layer and stimulus intensity. *J Neurosci* 24:3985–3998.
5. Nelson SB, Valakh V (2015) Excitatory/inhibitory balance and circuit homeostasis in autism spectrum disorders. *Neuron* 87:684–698.
6. Gao R, Penzes P (2015) Common mechanisms of excitatory and inhibitory imbalance in schizophrenia and autism spectrum disorders. *Curr Mol Med* 15:146–167.
7. Rutherford LC, DeWan A, Lauer HM, Turrigiano GG (1997) Brain-derived neurotrophic factor mediates the activity-dependent regulation of inhibition in neocortical cultures. *J Neurosci* 17:4527–4535.
8. Uezu A, et al. (2016) Identification of an elaborate complex mediating postsynaptic inhibition. *Science* 353:1123–1129.
9. Lu W, Bushong EA, Shih TP, Ellisman MH, Nicoll RA (2013) The cell-autonomous role of excitatory synaptic transmission in the regulation of neuronal structure and function. *Neuron* 78:433–439.
10. Xue M, Atallah BV, Scanziani M (2014) Equalizing excitation-inhibition ratios across visual cortical neurons. *Nature* 511:596–600.
11. Gu X, Zhou L, Lu W (2016) An NMDA receptor-dependent mechanism underlies inhibitory synapse development. *Cell Rep* 14:471–478.
12. Gibson JR, Huber KM, Südhof TC (2009) Neuroligin-2 deletion selectively decreases inhibitory synaptic transmission originating from fast-spiking but not from somatostatin-positive interneurons. *J Neurosci* 29:13883–13897.
13. Budreck EC, Scheiffele P (2007) Neuroligin-3 is a neuronal adhesion protein at GABAergic and glutamatergic synapses. *Eur J Neurosci* 26:1738–1748.
14. Varoqueaux F, Jamain S, Brose N (2004) Neuroligin 2 is exclusively localized to inhibitory synapses. *Eur J Cell Biol* 83:449–456.
15. Shipman SL, et al. (2011) Functional dependence of neuroligin on a new non-PDZ intracellular domain. *Nat Neurosci* 14:718–726.
16. Bartley AF, Huang ZJ, Huber KM, Gibson JR (2008) Differential activity-dependent, homeostatic plasticity of two neocortical inhibitory circuits. *J Neurophysiol* 100:1983–1994.
17. Felts PA, Yokoyama S, Dib-Hajj S, Black JA, Waxman SG (1997) Sodium channel alpha-subunit mRNAs I, II, III, NaG, Na6 and hNE (PN1): Different expression patterns in developing rat nervous system. *Brain Res Mol Brain Res* 45:71–82.
18. Qiao X, Werkman TR, Gorter JA, Wadman WJ, van Vliet EA (2013) Expression of sodium channel α subunits 1.1, 1.2 and 1.6 in rat hippocampus after kainic acid-induced epilepsy. *Epilepsy Res* 106:17–28.
19. Levy JM, Chen X, Reese TS, Nicoll RA (2015) Synaptic consolidation normalizes AMPAR quantal size following MAGUK loss. *Neuron* 87:534–548.
20. Goold CP, Nicoll RA (2010) Single-cell optogenetic excitation drives homeostatic synaptic depression. *Neuron* 68:512–528.
21. Ibata K, Sun Q, Turrigiano GG (2008) Rapid synaptic scaling induced by changes in postsynaptic firing. *Neuron* 57:819–826.
22. Thiagarajan TC, Lindskog M, Tsien RW (2005) Adaptation to synaptic inactivity in hippocampal neurons. *Neuron* 47:725–737.
23. Bezaire MJ, Soltesz I (2013) Quantitative assessment of CA1 local circuits: Knowledge base for interneuron-pyramidal cell connectivity. *Hippocampus* 23:751–785.
24. Straub C, Granger AJ, Saulnier JL, Sabatini BL (2014) CRISPR/Cas9-mediated gene knock-down in post-mitotic neurons. *PLoS One* 9:e105584.
25. Incontro S, Asensio CS, Edwards RH, Nicoll RA (2014) Efficient, complete deletion of synaptic proteins using CRISPR. *Neuron* 83:1051–1057.
26. Sakurada K, Masu M, Nakanishi S (1993) Alteration of Ca2+ permeability and sensitivity to Mg2+ and channel blockers by a single amino acid substitution in the N-methyl-D-aspartate receptor. *J Biol Chem* 268:410–415.
27. Yasuda R, Sabatini BL, Svoboda K (2003) Plasticity of calcium channels in dendritic spines. *Nat Neurosci* 6:948–955.
28. Davare MA, et al. (2001) A β2 adrenergic receptor signaling complex assembled with the Ca2+ channel Cav1.2. *Science* 293:98–101.
29. Földy C, Malenka RC, Südhof TC (2013) Autism-associated neuroligin-3 mutations commonly disrupt tonic endocannabinoid signaling. *Neuron* 78:498–509.
30. Nguyen QA, Horn ME, Nicoll RA (2016) Distinct roles for extracellular and intracellular domains in neuroligin function at inhibitory synapses. *Elife* 5:e19236.
31. Chanda S, Hale WD, Zhang B, Wernig M, Südhof TC (2017) Unique versus redundant functions of neuroligin genes in shaping excitatory and inhibitory synapse properties. *J Neurosci* 37:6816–6836.
32. Somogyi P, Klausberger T (2005) Defined types of cortical interneurone structure space and spike timing in the hippocampus. *J Physiol* 562:9–26.
33. Jiang X, et al. (2015) Principles of connectivity among morphologically defined cell types in adult neocortex. *Science* 350:aac9462.
34. Miao C, Cao Q, Moser MB, Moser EI (2017) Parvalbumin and somatostatin interneurons control different space-coding networks in the medial entorhinal cortex. *Cell* 171:507–521.e17.
35. Pinto L, Dan Y (2015) Cell-type-specific activity in Prefrontal cortex during goal-directed behavior. *Neuron* 87:437–450.
36. Funk CM, et al. (2017) Role of somatostatin-positive cortical interneurons in the generation of sleep slow waves. *J Neurosci* 37:9132–9148.
37. Kepecs A, Fishell G (2014) Interneuron cell types are fit to function. *Nature* 505:318–326.
38. Tremblay R, Lee S, Rudy B (2016) GABAergic interneurons in the neocortex: From cellular properties to circuits. *Neuron* 91:260–292.
39. Di Cristo G, et al. (2004) Subcellular domain-restricted GABAergic innervation in primary visual cortex in the absence of sensory and thalamic inputs. *Nat Neurosci* 7:1184–1186.
40. Villa KL, et al. (2016) Inhibitory synapses are repeatedly assembled and removed at persistent sites in vivo. *Neuron* 89:756–769.
41. Marsden KC, Shemesh A, Bayer KU, Carroll RC (2010) Selective translocation of Ca2+/calmodulin protein kinase IIalpha (CaMKIIalpha) to inhibitory synapses. *Proc Natl Acad Sci USA* 107:20559–20564.
42. Marsden KC, Beattie JB, Friedenthal J, Carroll RC (2007) NMDA receptor activation potentiates inhibitory transmission through GABA receptor-associated protein-dependent exocytosis of GABA(A) receptors. *J Neurosci* 27:14326–14337.
43. Petrini EM, et al. (2014) Synaptic recruitment of gephyrin regulates surface GABAA receptor dynamics for the expression of inhibitory LTP. *Nat Commun* 5:3921.
44. Schlick B, Flucher BE, Obermair GJ (2010) Voltage-activated calcium channel expression profiles in mouse brain and cultured hippocampal neurons. *Neuroscience* 167:786–798.
45. Kurotani T, Yamada K, Yoshimura Y, Crair MC, Komatsu Y (2008) State-dependent bidirectional modification of somatic inhibition in neocortical pyramidal cells. *Neuron* 57:905–916.
46. Peng Y-R, et al. (2010) Postsynaptic spiking homeostatically induces cell-autonomous regulation of inhibitory inputs via retrograde signaling. *J Neurosci* 30:16220–16231.
47. Nugent FS, Penick EC, Kauer JA (2007) Opioids block long-term potentiation of inhibitory synapses. *Nature* 446:1086–1090.
48. Alger BE, Pitler TA (1995) Retrograde signaling at GABAA-receptor synapses in the mammalian CNS. *Trends Neurosci* 18:333–340.
49. Zoghbi HY, Bear MF (2012) Synaptic dysfunction in neurodevelopmental disorders associated with autism and intellectual disabilities. *Cold Spring Harb Perspect Biol* 4:a009886.
50. Kuhse J, et al. (2012) Phosphorylation of gephyrin in hippocampal neurons by cyclin-dependent kinase CDK5 at Ser-270 is dependent on collybistin. *J Biol Chem* 287:30952–30966.
51. Körber C, et al. (2012) Effects of distinct collybistin isoforms on the formation of GABAergic synapses in hippocampal neurons. *Mol Cell Neurosci* 50:250–259.
52. Shipman SL, Nicoll RA (2012) A subtype-specific function for the extracellular domain of neuroligin 1 in hippocampal LTP. *Neuron* 76:309–316.
53. Stoppini L, Buchs PA, Muller D (1991) A simple method for organotypic cultures of nervous tissue. *J Neurosci Methods* 37:173–182.
54. Schnell E, et al. (2002) Direct interactions between PSD-95 and stargazin control synaptic AMPA receptor number. *Proc Natl Acad Sci USA* 99:13902–13907.
55. Gray JA, et al. (2011) Distinct modes of AMPA receptor suppression at developing synapses by GluN2A and GluN2B: Single-cell NMDA receptor subunit deletion in vivo. *Neuron* 71:1085–1101.